Available online at www.sciencedirect.com
SCIENCE DIRECT®
Cement & Concrete Composites 27 (2005) 399–411
Cement & Concrete Composites
www.elsevier.com/locate/cemconcomp

A detailed study of crack propagation in cement-based fibre composite beams under bending

Evelyne Toussaint, Jean-François Destrebecq *, Michel Grédiac

Laboratoire d'Etudes et de Recherches en Mécanique des Structures, Université Blaise Pascal Clermont II, 24, avenue des Landais, BP 206, 63174 Aubière Cedex, France

Received 10 March 2003; accepted 21 May 2004

Abstract

Multiple cracking of beams made of cement-based composite was extensively studied by means of a suitable non-contact measurement technique. Images of a grid-pattern bonded onto the surface of a tested specimen were captured by a digital camera. Image processing by means of an appropriate software provided the displacement field within the zone under investigation. Cracks were revealed by discontinuities in the displacement field. Results are presented for three specimens tested in three- or four-point bending. Location, actual length and width are easily and precisely determined for each of the cracks within the zone under investigation. High sensitivity, early crack detection and no need to anticipate crack location are among the main features of this full-field measurement method. Crack propagation is derived from crack diagrams obtained at successive loading levels. Initial length, spacing, opening, propagation and profile of cracks are discussed in terms of mode of loading and bond properties of the material.

Keywords: Cement-based fibre composite; Crack propagation; Full-field measurement; Grid method; Image analysis; Multi-cracking

1. Introduction

The last decades have seen many developments in the composition of cement composites which has led to significant improvements of their mechanical properties. Due to fibres, these composite materials present an interesting feature: they exhibit an elasto-plastic response instead of the brittle response of the plain matrix. Moreover, their mechanical properties can be tailored, within a certain range, to the requirements of the designers. Cracking and crack propagation are key issues to better understand the relationship between certain macroscopic mechanical properties and microstructure. Indeed, the cracks directly cause the degradation of the stiffness, and they directly influence the plastic part of the stress/strain response. Cracking has therefore been studied extensively in the literature, but suitable techniques are required to analyse this phenomenon. For instance, image analysis is an efficient tool to highlight microcracks and some microdefects which appear on the surface of the specimens under investigation either in two dimensions [1] or in three dimensions [2]. Such a technique is used to characterize microcracks, namely those cracks with width less than about 10 μm. Microcrack morphology in terms of width, profile, length, orientation or density can be determined with image analysis, but the use of a microscope is often required in this case. The size of the field to be analysed is therefore limited for obvious practical reasons.

Full-field measurement techniques such as holographic interferometry [3], speckle [4], grid method [5]

* Corresponding author. Fax: +33 4 73 40 74 94.
E-mail address: destrebecq@cust.univ-bpclermont.fr (J.-F. Destrebecq).

0958-9465/$ - see front matter © 2004 Elsevier Ltd. All rights reserved.
doi:10.1016/j.cemconcomp.2004.05.003

and image intercorrelation [6] provide larger field information. They are therefore suitable for studying heterogeneous materials. In a pioneering work, Dantu [7] measured stress and strain variations in concrete under compression covered with photoelastic coating, but experimental results were processed by hand. Nowadays full-field measurement techniques are coupled with image acquisition by a camera and computerized image processing, leading to efficient tools which can be used to investigate heterogeneous materials and to characterize macrocracks with widths of some tens of micrometers and length of some millimeters. Displacement contours are thus available over a large part of the surface of the specimen *during* a mechanical test. For instance, this feature has been used to analyse the fracture process zone ahead of a crack tip in concrete [8]. A crack appears as a discontinuity in the displacement field. It can be detected provided that its width is greater than the resolution of the method, which depends in practice on several parameters among which are the size of the field, the sensitivity of the camera, and the capabilities of the programme that processes the images. In conclusion, full-field techniques are well suited to study cracking and crack propagation.

Such a technique has been used in the present work to investigate cracked zones in beams made of cement-based fibre composites and loaded in three- or four-point bending. The experimental procedure and the tested specimens are described in the first part of the paper. Results in terms of crack characterization are then presented and discussed. The results highlight the capabilities of full-field measurement techniques to obtain relevant information on the cracking response of cement-based composites.

2. Experimental set-up

2.1. Specimens and materials under investigation

A series of beams were tested under three- and four-point bending. The specimens were made of a *Ductal*® fibre reinforced cementitious composite. This ultra high performance material is expected to exhibit elevated strength and high ductility in compression and tension. It is made of a special cementitious matrix reinforced with metallic fibres. The maximum size of the aggregates does not exceed 0.5 mm, while the fibres are 0.2 mm in diameter and 13 mm in length.

Two types of materials exhibiting different mechanical properties were studied. The cementitious matrix of the first material (called hereafter "Material 1") was optimized in terms of rheological properties. The constitution of the matrix of the second ("Material 2") was purposely modified to reduce the bond conditions between fibres and cementitious matrix, and therefore modify the cracking properties of the composite. The fibre volume fraction was about 2% (160 kg/m^3) and the fibres were randomly distributed in the fresh mixture during preparation. The specimens were prepared and provided by the Lafarge Research Center. No more information was available about specimen preparation.

Table 1
Types of tests and specimens

Specimen	Material	Type of test	Notch
A	1	Four-point bending	None
B	1	Three-point bending	$1 \times 10\,mm^2$
C	2	Four-point bending	None

The specimens were 280 mm long, and 70 mm × 70 mm square in cross-section. A 10 mm × 1 mm initial notch was machined beforehand in the specimens to be tested in three-point bending. The objective in this case was to initiate and to concentrate the cracks in the mid-span region of the specimens. The difference between the mechanical responses of both materials was expected to be detected and characterized using a full-field measurement technique. The types of tests and specimens are listed in Table 1.

2.2. Full-field measurement technique and preparation of the specimens

The technique used in the present study is based on the grid method developed by Surrel [5,9]. It involves the analysis of the deformation of a grid bonded onto the surface of a specimen under test. It requires a digital camera which captures images of the deformed grid at specified levels of loading of the specimen. The images are stored in a computer. Image-files are finally processed by means of an appropriate software in order to obtain the displacement field of the zone under investigation. The software, called *Frangyne*, was also developed by Surrel [10]. It is suited to the detection of very small variations of the pitch of the grid caused by a deformation of the surface. The principle of this method has been described in recent papers (see Ref. [11] for instance). It is therefore not reviewed here.

The specimens were prepared as follows. A transferable grid pattern of *Mecanorma* type was first bonded onto one external side surface of the specimen to be tested. The pitch of the grid was 0.571 mm. The size of the grid was 120 mm × 70 mm (120 mm × 60 mm for notched beams) as shown in Fig. 1. Since the cracks were expected to be roughly vertical, the grids were bonded in such a way that the stripes were perpendicular to the longitudinal axis of the beam in order to measure the longitudinal component of the displacement field. A crack induces a discontinuity in the longitudinal displacement (called hereafter x-displacement), which can

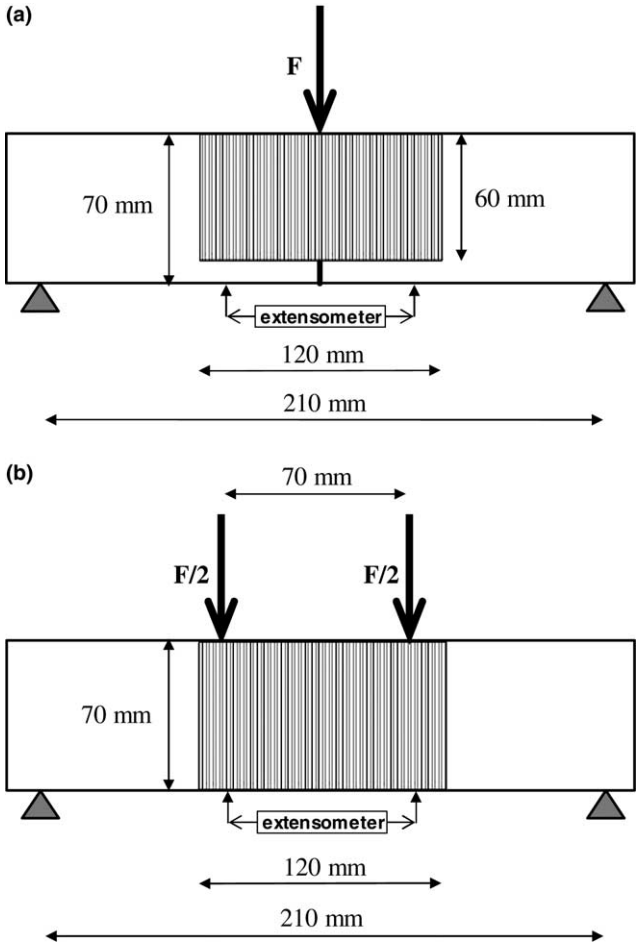

Fig. 1. Experimental set-up—location and size of the grids on the specimens: (a) three-point bending notched specimen and (b) four-point bending specimen.

be detected if the width of the crack, which is in fact the magnitude of the discontinuity, is greater than the resolution of the method. The resolution is about 9×10^{-6} m in the present case.

The procedure used for transferring the grid was very similar to the procedure described in Ref. [12] for bonding grids onto a foamed core sandwich beam. The concrete surface was first coated with a very thin coat of special filler paste suitable for smoothing surfaces in order to eliminate voids and irregularities. The surface was then covered with a thin layer of white paint using an atomizer to increase the contrast between the black stripes of the grid and the white painted surface. The grid was finally transferred and glued onto the painted surface of the specimen. It was assumed that the paste and the paint did not disturb the detection and the measurement of the cracks during the tests. This assumption was acceptable since the paste was soft and brittle and the paint layer was very thin. Full details concerning the transferring technique can be found in Ref. [12].

2.3. Test arrangement

Test results are reported for three beams tested under three- and four-point bending (Fig. 1). The material of each of these three specimens and the configuration used to test them are those listed above in Table 1. Three-point bending is simple to carry out but the effects are concentrated directly under the load and this small portion of material is not necessarily representative of the tested element. This configuration is however often used to test notched specimens, for example to estimate the fracture behaviour of cementitious composites [13]. Four-point bending is considered to better reflect the bending conditions in the central part of the element where pure bending without shearing is created.

The specimens were loaded by means of a Zwick testing machine. The tests were carried out at a constant rate of displacement of the loading point equal to 0.05 mm/min. An extensometer was fixed on the bottom of the specimen, in order to measure the overall stretch of the tensile face of the beam under test. The distance between the arms of the extensometer was 100 mm, and the relative displacement between the two arms is denoted u in the following sections. In practice, as soon as cracks had formed, the increase in u was mainly due to the opening of the cracks since the tensile deformation of the concrete blocks between consecutive cracks remained limited. Images of the deformed grids were regularly captured by a 10^6 pixel-CCD camera and stored during the tests. About 40–50 images of the deformed grid were captured during each test and processed afterwards.

It must be finally emphasized that full-field measurements provide a large amount of data which must be processed with suitable procedures. Only typical results obtained for three specimens are presented and discussed herein for the sake of clarity.

3. Detection and measurement of the cracks

3.1. Image acquisition

During the four-point bending tests (specimens *A* and *C*), two images were first captured at 10 kN and 20 kN respectively. Images were then captured every 3 kN up to the peak-load. After the peak, images were captured for every increase of 0.05–0.1 mm in the displacement u measured by the extensometer. The tests were stopped when the measurement capability of the extensometer ran out, i.e. $u = 2$ mm.

The image acquisition was more frequent during the three-point bending test (specimen *B*), since the maximum load was expected to be lower in this case. Up to the peak, images were captured and stored every 2–3 kN. After the peak, the frequency was the same as for four-point bending tests.

3.2. Locations and extensions of the cracks

Fig. 2a represents an example of a field of longitudinal displacement obtained with the grid method. The gray levels correspond to different magnitudes of the longitudinal displacement processed from images of the deformed grid within the zone of investigation. Discontinuities that may be seen in this diagram reveal the existence of three cracks. Fig. 2b represents the magnitude of the longitudinal component of the displacement along a given horizontal XX' axis. Each of the three "jumps" in this figure corresponds to a crack. In practice, the location of a crack is given by the abscissa of the corresponding jump. By repeating this procedure for a set of horizontal axes equally distributed throughout the depth of the specimen, it is possible to obtain a precise description of the complete crack pattern within the zone under investigation at a given level of loading. This was done for each of the three specimens by repeating this procedure every 5 mm from the bottom to the top of the grid.

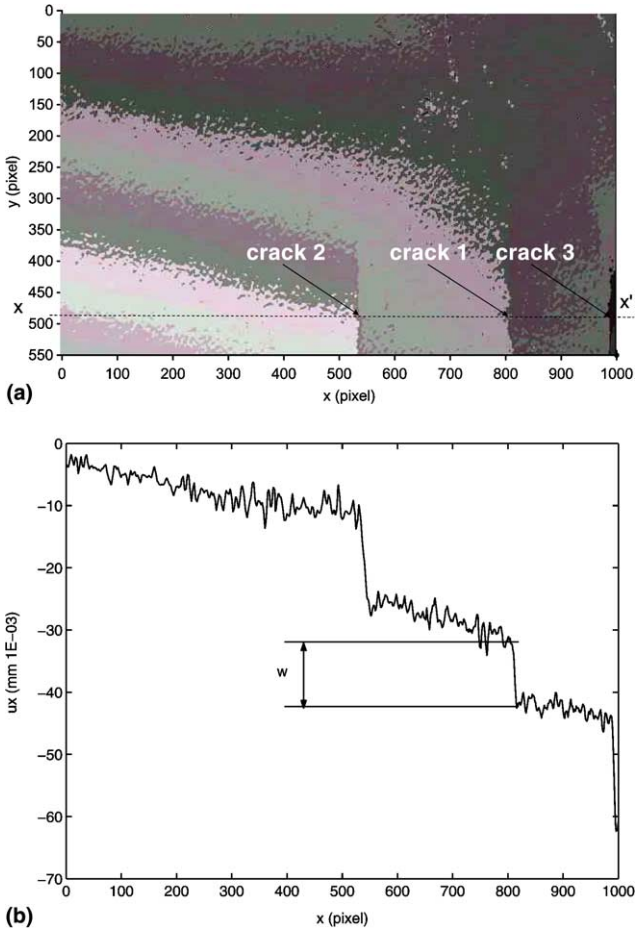

Fig. 2. Typical displacement field—crack detection and measurement—specimen C, $F = 33.0$ kN (pre-peak): (a) mapped longitudinal displacement in gray-level scale and (b) longitudinal displacement along axis XX'.

3.3. Widths and profiles of the cracks

The width of a given crack is equal to the magnitude of the corresponding jump in the longitudinal displacement field (illustrated in Fig. 2b for the second crack). This method was used to measure carefully the opening of the whole set of cracks at the lower edge of specimens A and C for all intermediate values of the loading. Results are discussed below in the relevant sections.

By repeating this method at different levels within the zone shown in Fig. 2a, it is possible to estimate the width distribution of a given crack along its length, that is the profile of the crack at a given level of loading. Because of the large amount of data, this procedure was applied only for some selected cracks, as will be shown below.

Note finally that the displacement field is obviously noisy. This leads to some uncertainty in this type of measurement, which is about 5 μm.

4. Analysis of the cracking process of the specimens

4.1. Introduction

The procedure described in Sections 3.1 and 3.2 for detecting cracks was used for every image stored during the tests. Early detection of new cracks was made possible due to the high sensitivity of the method. Moreover, it was not necessary to anticipate the locations of new cracks for their detection. Therefore, intensity of the loading force, location, initial length and width could be precisely determined for any new crack appearing within the zone under investigation. Similarly, propagation of existing cracks could be observed by comparing crack diagrams obtained at consecutive loading steps. The only limitation was the interval in loading between consecutive image acquisitions. Results obtained for the three selected specimens are presented below. Because of the large amount of data, only typical crack diagrams are shown in this section.

4.2. Specimen A

Fig. 3 represents the F/u curve recorded during the test. The plotted marks correspond to image acquisitions. Each number in this figure corresponds to a new crack. It shows when the crack was detected for the first time. Cracks are numbered in order of appearance.

Fig. 4a shows the crack pattern in the central zone of specimen A after the beginning of the cracking process, immediately after the appearance of crack 5 ($F = 39$ kN, $u = 0.09$ mm). Fig. 4b shows the crack pattern at the peak ($F = 71$ kN, $u = 1.12$ mm), when all of the cracks had formed. Fig. 4c represents the crack pattern just before the test was stopped ($F = 53$ kN, $u = 1.90$ mm).

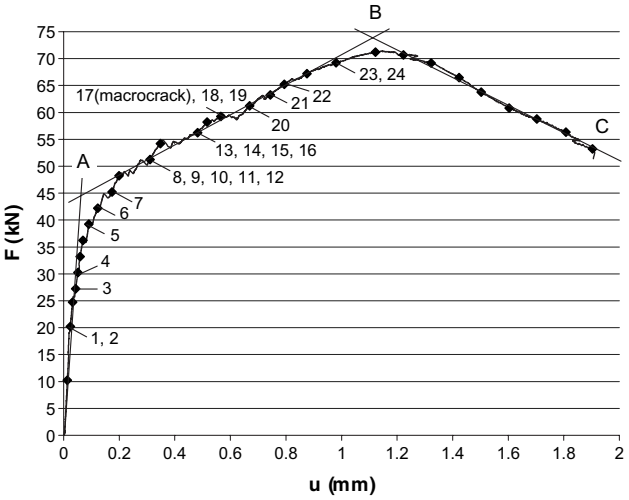

Fig. 3. *F*/*u* curve, specimen *A*.

According to Figs. 3 and 4, the behaviour of specimen *A* may be analysed in three stages:

- The first stage (*OA*) of the plot corresponds to the beam in its un-cracked stage. The first crack was detected at $F = 20\,\text{kN}$. On close inspection of Fig. 3, a slight drop in the load/displacement curve occurs at $F = 18.9\,\text{kN}$. This is probably the value of the load at which this first crack appeared.
- The second stage (*AB*) of the plot corresponds to the progressive cracking of the beam with the increase of the loading. Comparison of Fig. 4a and b shows that the density of cracks has dramatically increased during this stage. The sharp decrease in the slope of the curve indicates a significant loss of stiffness of the beam, due to the extensive cracking of its tensile zone.
- Comparison of Fig. 4b and c shows that the crack pattern had remained almost unchanged after the peak: no new crack formed during the third stage (*BC*) and existing cracks did not propagate further. Crack 17 became a macrocrack and continued to open dramatically until the test was stopped.

More generally, several points are worth noting from Fig. 4:

- Cracks were regularly distributed within the investigated zone, showing a pure bending state of stress between the two loading points.
- On the whole, cracks did not appear or extend smoothly. Most of them propagated immediately after they had appeared. They often exhibited a significant length, called hereafter "initial length", when they were detected for the first time. This can be seen with crack 5, just formed in Fig. 4a. This "initial length" (l_{initial}) is plotted in Fig. 5 for all cracks.

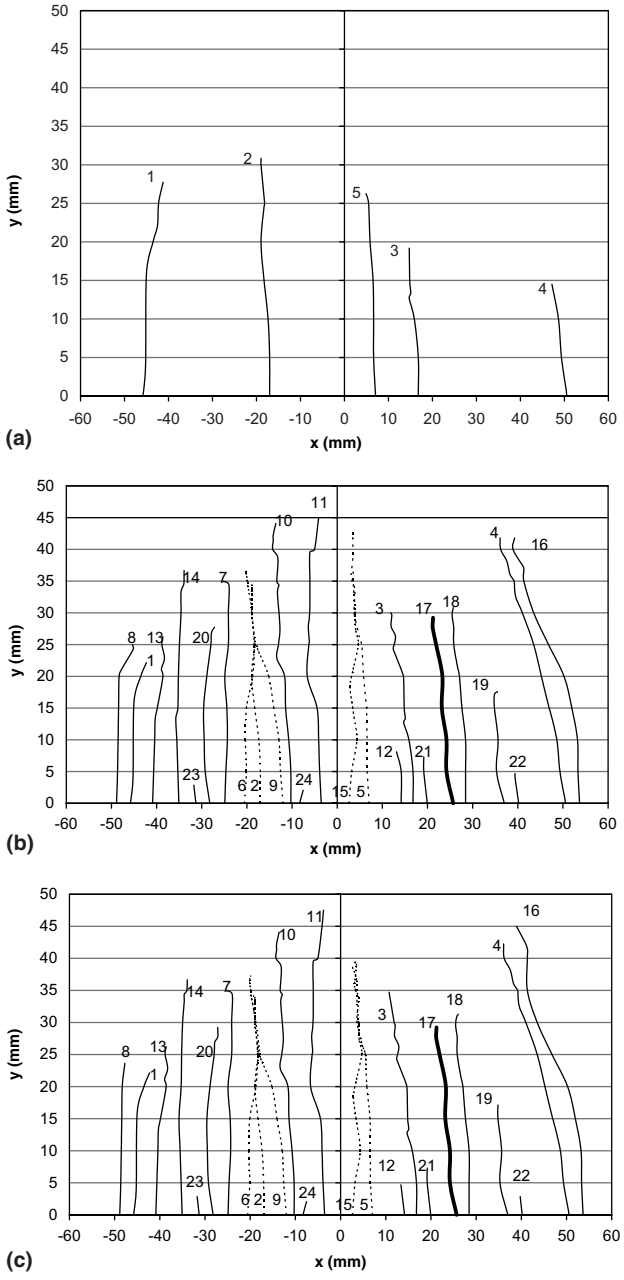

Fig. 4. Crack pattern at three different loading stages, specimen *A*: (a) $F = 39\,\text{kN}$, $u = 0.09\,\text{mm}$ (pre-peak); (b) $F = 71\,\text{kN}$, $u = 1.12\,\text{mm}$ (peak); (c) $F = 53\,\text{kN}$, $u = 1.90\,\text{mm}$ (test end).

Up to the appearance of the main crack (crack 17), l_{initial} tended to increase as the loading *F* increased, showing a cracking activity which increased with *F*. The macrocrack appeared at $F = 59\,\text{kN}$ and $u = 0.56\,\text{mm}$, that is 83% of the maximum load. Some additional cracks appeared after that point, but their "initial length" was smaller. This was especially the case for the last cracks formed (cracks 21–24).

- Cracks generally extended during the test, excepted crack 1 which partially closed for $F \geqslant 65\,\text{kN}$ (compare Fig. 4a and b). Some cracks extended beyond

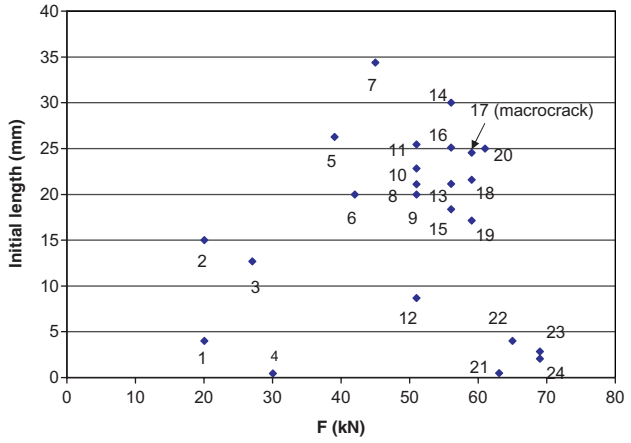

Fig. 5. Initial length of the cracks, specimen *A*.

$y = h/2$, that is beyond the initial level of the neutral axis in the un-cracked specimen. Only few cracks remained short during the test.

- Some cracks coalesced: cracks 2, 6, 9 at $x = -18$ mm and cracks 5, 15 at $x = 4$ mm (Fig. 4b). It has been observed on another specimen of the same series that some cracks coalesced and then separated again.
- Comparing Fig. 4b and c shows that the length of the cracks remained approximately constant near and after the peak. Hence the additional deflection after the peak was mainly caused by the opening of the existing cracks (especially the macrocrack) rather than by some new cracks.

The number N of cracks that appeared in the central zone of specimen A vs both the displacement u and the load F is plotted in Fig. 6a and b respectively. Fig. 6a shows a fairly linear relationship between the number of cracks and the lengthening of the tensile face of the specimen, until the final value $N = 24$ was reached. The shape of the curve N vs F in Fig. 6b is very different. N first increased slowly during the first stage ($0 \leqslant F \leqslant 30$ kN) where only three cracks formed. It then rose dramatically during the second stage until the peak was reached ($F = 71$ kN), and remained finally constant after the peak. This shows a critical response of the specimen in terms of cracking during the second stage of the curve, especially when $40\,\text{kN} \leqslant F \leqslant 60\,\text{kN}$.

The cracking pattern measured on the specimen made of the same material, but subjected to three-point bending, will now be examined.

4.3. Specimen B

The behaviour of the notched specimen tested in three-point bending was different from the previous specimen tested in four-point bending. Observing Figs. 7–9, the main differences may be listed as follows:

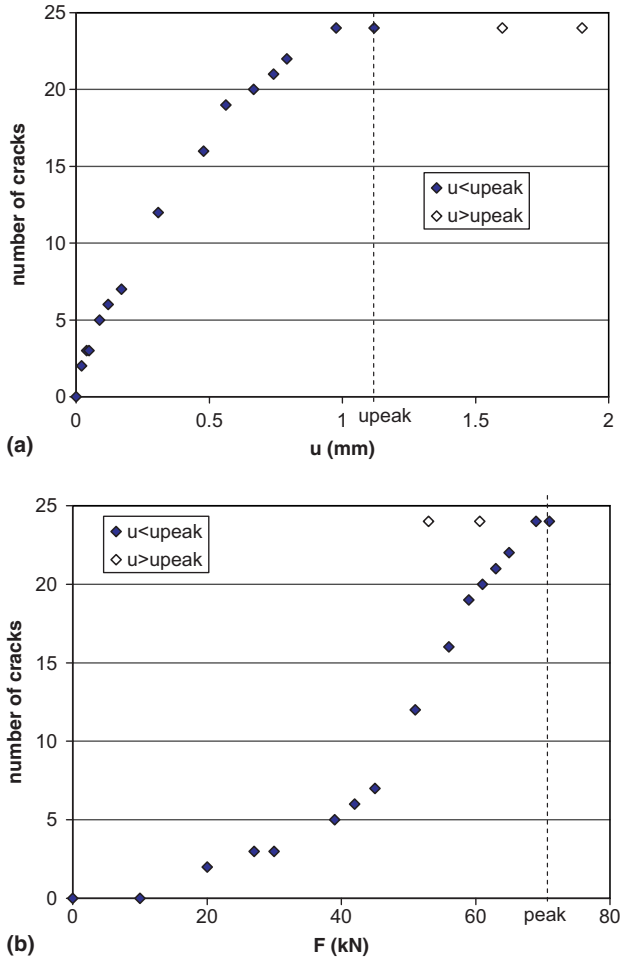

Fig. 6. Number of cracks N vs u and F, specimen *A*.

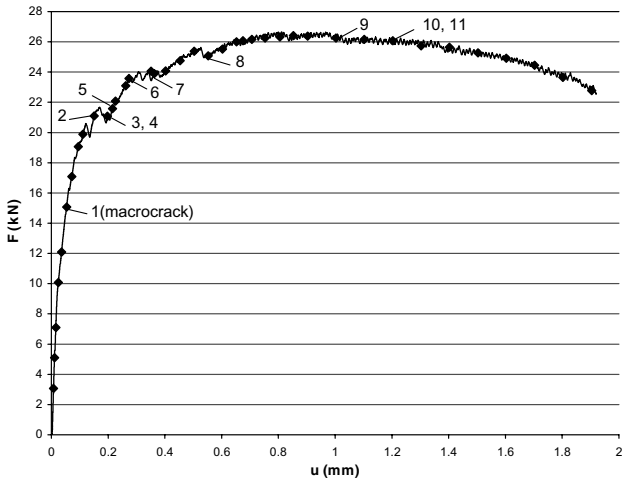

Fig. 7. *F*/*u* curve, specimen *B*.

- The shape of the *F*/*u* curve is very different. Compared with the first stage, the length of the second stage is much shorter for specimen *B* than for specimen *A*. The peak value of the loading force was about

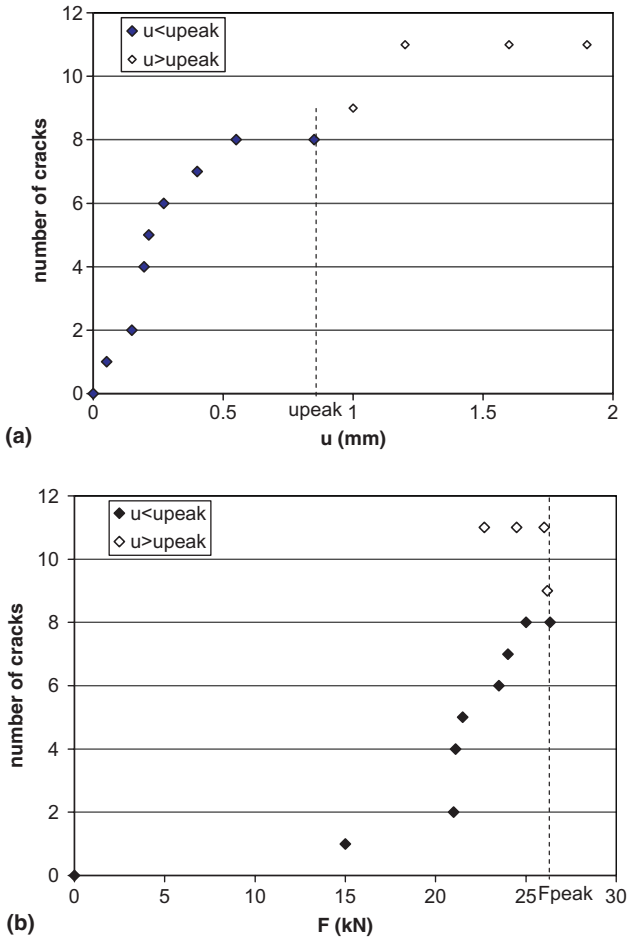

Fig. 8. Number of cracks N vs u and F, specimen B.

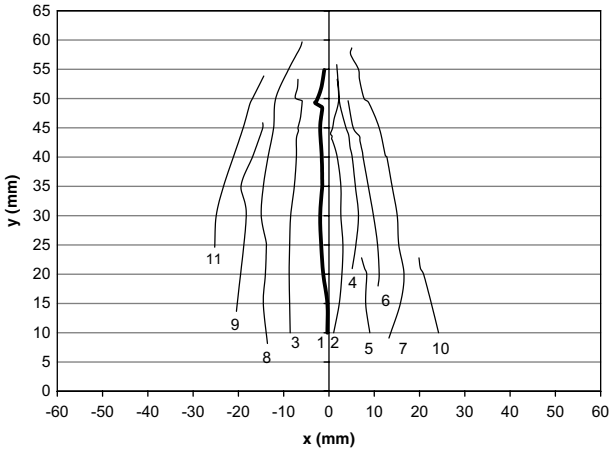

Fig. 9. Specimen B—example of crack pattern at $F = 24.5\,\text{kN}$.

37% of that obtained in four-point bending, that is a maximum value of the bending moment about 56% that of specimen A. After the peak, the reduction in the load proved much lower than for the previous specimen.

- The first crack to form proved to be the main one. Its initial length was 26 mm instead of 15 mm for crack 1 in specimen A, and was first detected at $F = 15\,\text{kN}$. This meant that the crack formed between $F = 12\,\text{kN}$ and $F = 15\,\text{kN}$, since it was not detected at $F = 12\,\text{kN}$. Therefore, the value of the cracking moment might be estimated between 0.63 kN m and 0.79 kN m. Compared with that of specimen A (0.66 kN m), the value of the cracking moment of specimen B was between 95% and 120% that of specimen A.
- The total number of cracks N was lower in this case, since only 11 cracks were detected instead of 24 in four-point bending. As for the previous case, the increase of N vs u is more progressive than for N vs F. The curve in Fig. 8a is similar to that in Fig. 6a except the final value of N. Most of the cracking activity was concentrated for $21\,\text{kN} \leqslant F \leqslant 25\,\text{kN}$. This is clearly highlighted in Fig. 8b where N has been plotted vs F. Contrary to the preceding case, the number of cracks continued to increase after the peak since three additional cracks appeared beyond u_{peak}.
- A typical crack pattern is presented in Fig. 9 for $F = 24.5\,\text{kN}$ and $u = 1.60\,\text{mm}$ (after the peak). This pattern is somewhat different from the multiple cracks patterns shown in Fig. 4, and illustrates the relationship between the mode of loading and the cracking activity. In the present case, the macrocrack (crack 1) had formed in the notched cross-section of the beam, and had already become a macrocrack at this stage. All the cracks formed and propagated in a narrow strip adjacent to the initial notch.
- Note that experimental data are not available below the tip of the notch since the grid was bonded above. It clearly appears however that some cracks did not extend to the bottom of the grid, hence they did not extend beyond the zone under investigation. The same coalescence phenomenon as observed previously can be observed with cracks 2 and 4.

4.4. Specimen C

The crack pattern obtained with Material 2 under four-point bending is now examined. The F/u curve is plotted in Fig. 10. The mechanical response of specimen C was different from the response of specimen A:

- The shape of the F/u curves was somewhat different. The peak value of the loading force was lower in the present case: 61.1 kN for specimen C instead of 71.0 kN for specimen A. During the second stage, the slope was much stiffer for specimen C than for specimen A. Moreover, specimen C exhibited a large

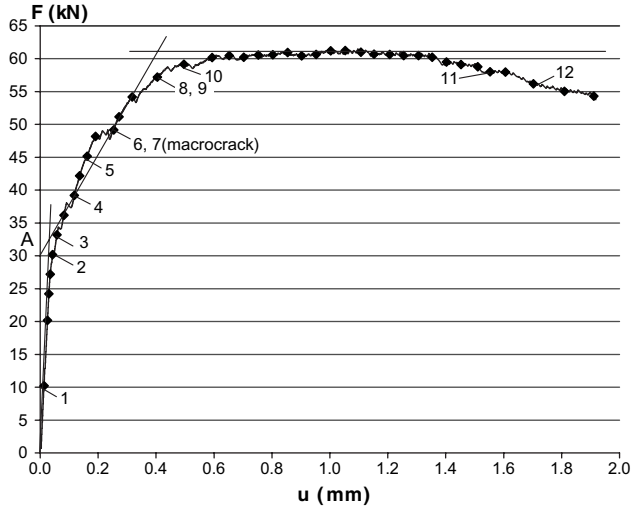

Fig. 10. *F*/*u* curve, specimen *C*.

"plastic" response with only a small decrease of the loading force at the end of the test. This meant that the tensile zone was stretching at a nearly constant load during most of the third stage.

- It is worth noting that the number of cracks remained constant for $0.49\,\text{mm} \leqslant u \leqslant 1.51\,\text{mm}$, when the applied loading remained approximately constant. This meant that the increase in deflection during the third stage was mainly due to the opening of existing cracks.
- The cracking processes in specimens *C* and *A* were different. The first crack was detected at $F = 10\,\text{kN}$ (instead of 18.9 kN for specimen *A*). Its initial length was 10 mm (15 mm for specimen *A*). The number of cracks in specimen *C* was half the number of cracks in specimen *A*, showing a lower cracking activity in the present case. From this point of view, specimen *C* may be compared to specimen *B*.
- Fig. 11a shows that most of the cracks had appeared for $u \leqslant 0.49\,\text{mm}$ in specimen *C*, whereas an equivalent situation was reached in specimen *A* at $u = 0.98\,\text{mm}$ (see Fig. 6a).
- Most of the cracks appeared in specimen *C* for $F \geqslant 30\,\text{kN}$ (Fig. 11b), whereas the cracking process was more progressive in specimen *A* (Fig. 6b). Another difference between the two specimens is the fact that two new cracks (11 and 12) formed after the peak in specimen *C*, whereas all the cracks had already appeared before the peak in specimen *A*.

The initial length of the cracks is plotted in Fig. 12. Contrary to specimen *A*, the initial length of the cracks was continuously increasing even after the macrocrack had already formed. The global trend was that the initial length increased as the applied loading increased during the test.

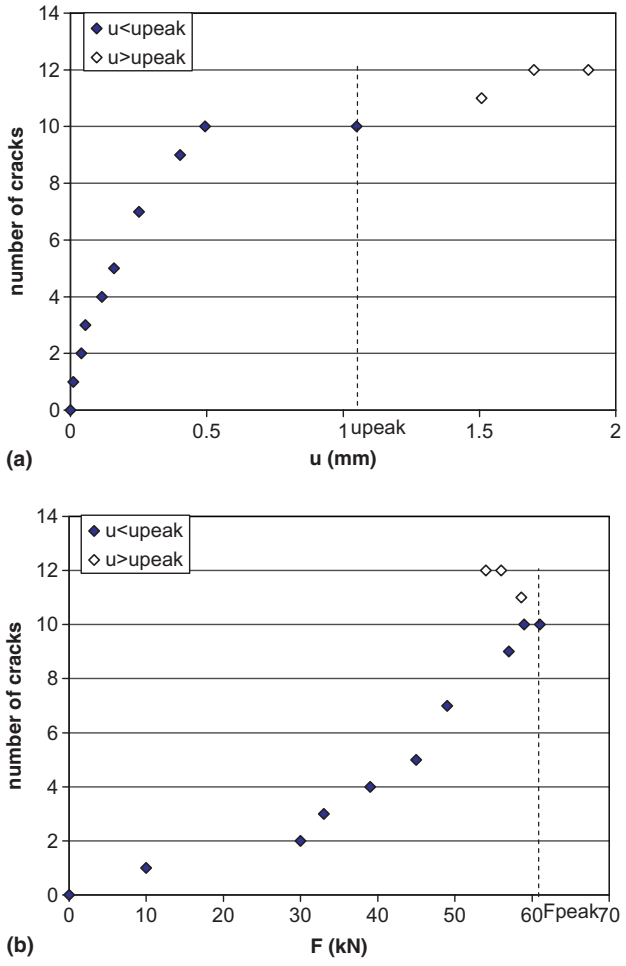

Fig. 11. Number of cracks *N* vs *u* and *F*, specimen *C*.

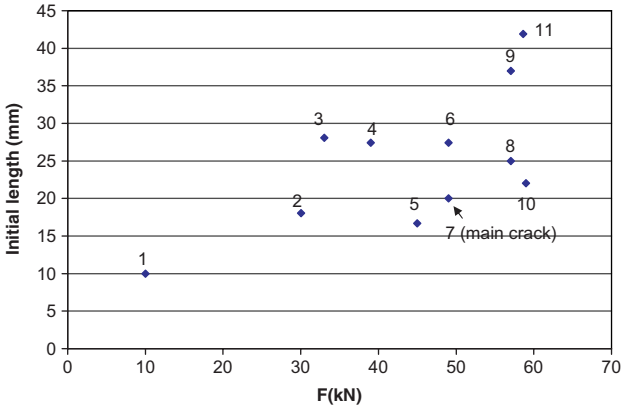

Fig. 12. Initial length of the cracks, specimen *C*.

4.5. Conclusion

A detailed analysis of the multiple cracking of the specimens was made possible by using a full-field measurement method. The crack patterns were very different between the two materials, and between the two types of

tests. It was concluded that the bond conditions between metallic fibres and cementitious matrix has a strong influence on the cracking activity, and therefore on the mechanical response of the specimens.

5. Analysis of cracks widths

5.1. Introduction

The width of the cracks is an important information to describe the cracking process in a cement-based composite. For instance, a typical method for characterizing the cracking behaviour of composite elements is based on the measurement of displacements at the mouth of an initial notch subjected to mode I of cracking [14]. Without an initial notch, such measurements cannot easily be performed with an extensometer since the locations of the cracks are not known before testing. One of the features of full-field measurements is to allow the measurement of the openings of the cracks whatever their locations in the area under investigation.

Several types of measurements have been performed on specimens *A* and *C*. Typical results are presented in the following sections. Firstly, the crack mouth opening displacement has been measured at the bottom edge of the specimens at two loading values: at peak-load and after the peak just before termination of the test. Secondly, the evolution of the opening of the macrocrack and of the four closest cracks during the test is presented. Finally, the profile of the cracks is plotted.

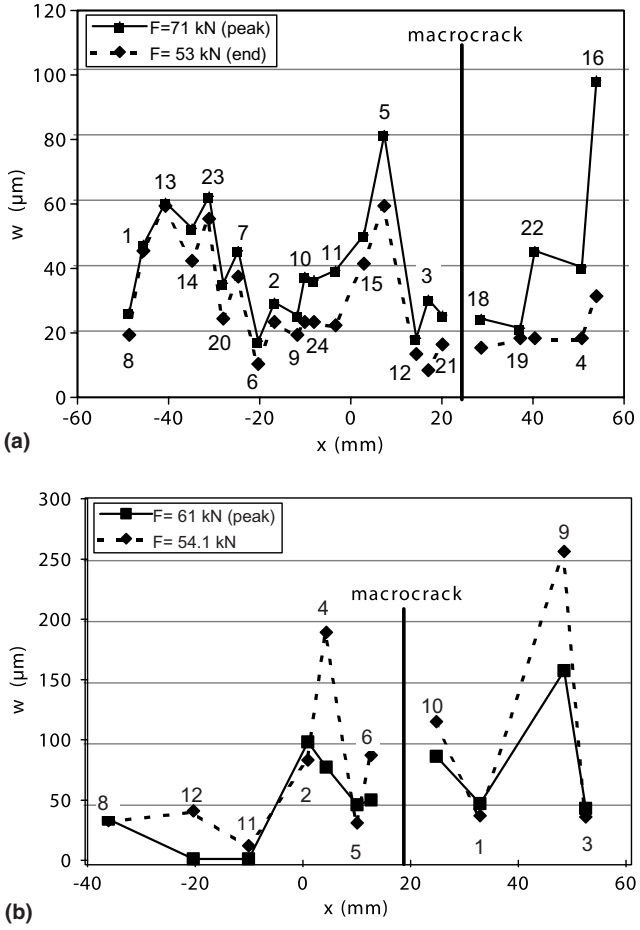

Fig. 13. Width *w* of the cracks at the bottom edge of specimens *A* (a) and *C* (b).

5.2. Crack width distributions in specimens A and C

5.2.1. Specimen A

The widths *w* of the cracks at the bottom edge of specimen *A* are plotted in Fig. 13a at two loading stages: the peak ($F = 71.0$ kN) and the end of the test ($F = 53.0$ kN). For the sake of clarity, the macrocrack is not reported in this figure since its width is much greater than the other ones. At $F = 71.0$ kN, *w* is randomly distributed between 10 μm and 100 μm with an average value $\bar{w}$ equal to 41 μm. It is worth noting that the crack width decreases after the peak, as illustrated by the dotted line in Fig. 13a. As a matter of fact, this trend is related to the sharp decrease in the loading force during the third stage of the curve (see Fig. 3). Thus, this confirms that the increase in *u* during this stage was only caused by the macrocrack which continued to open after the peak.

5.2.2. Specimen C

Fig. 13b represents the crack widths at the bottom edge of specimen *C* at peak-load ($F = 61.1$ kN) and at test end ($F = 54.1$ kN). The width of cracks is also randomly distributed in this case, but the distribution is obviously asymmetrical in the present case. This is due to larger crack spacing in the right half of the sample. As a matter of fact, the total number of cracks in specimen *C* was half that in specimen *A*, leading to wider crack opening. Contrary to the preceding case, the crack widths in specimen *C* were generally greater at the end of test (dashed line) than at peak-load (solid line): the average opening $\bar{w}$ was 70 μm at the peak and 83 μm at the end of the test. Thus, it may be concluded that the increase in *u* during the third stage was caused by the on-going opening of all cracks but not only the macrocrack, contrary to specimen *A*. This highlights a difference in the mechanical responses of specimens *A* and *C*. It is generally assumed that lower bond strength between steel and concrete leads to larger crack spacing and wider crack opening [15]. This was actually the case in specimen *C* where bond properties of Material 2 had been purposely reduced (see Section 2.1). The comparison of the cracking activities observed in specimens *A* and *C* by means of the full-field measurement method is in fair agreement with this well known observation.

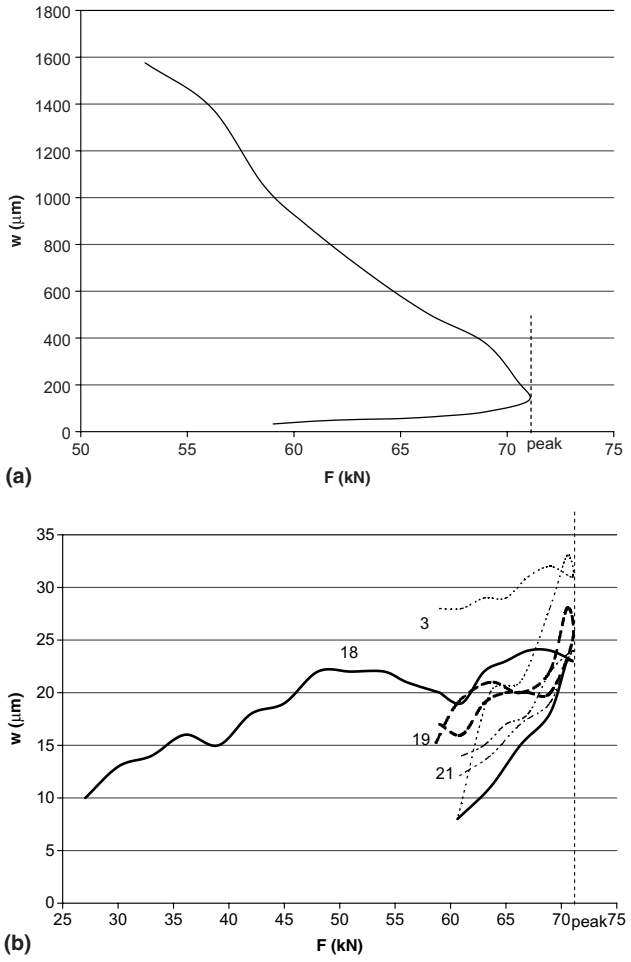

Fig. 14. Width of cracks measured at the bottom edge of specimen *A*: (a) width of macrocrack 17 and (b) width of cracks 3, 18, 19 and 21.

5.3. Interaction between macrocrack and neighbouring cracks

5.3.1. Specimen A

The width w of the macrocrack vs the loading F is plotted in Fig. 14a. The width of the four cracks closest to the macrocrack (cracks 3 and 21 on the left hand side, cracks 18 and 19 on the right hand side) are plotted in Fig. 14b. The width of the macrocrack 17 was from the outset larger than the width of the other cracks. Also, the rate of opening was higher for the macrocrack than for the other ones. At peak-load, the width of the macrocrack was about 150 μm, whereas the width of the others ranged between 22 μm and 31 μm. Thus, it may be concluded that crack 17 behaved as a main crack from its earliest appearance. It turned to a macrocrack when the peak was reached: its width dramatically increased after the peak, whereas the widths of cracks 3, 18, 19 and 21 decreased during this third stage. Note finally that the macrocrack formed suddenly and its exhibited a significant initial length, as reported in the first row in Table 2.

Table 2
Main features of the macrocracks (F: load at macrocrack appearance)

Specimen	F/F_{peak} (%)	Initial length (mm)	Final length (mm)
A	83.1	24.6	29.4
B	57.0	25.7	45.3
C	80.2	20.0	42.3

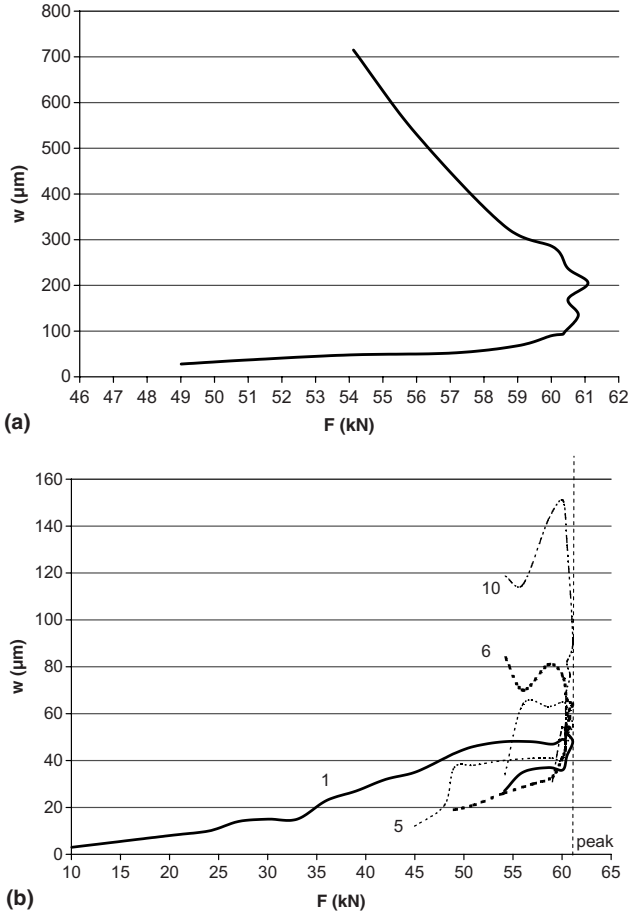

Fig. 15. Width of cracks measured at the bottom edge of specimen *C*: (a) width of macrocrack 7 and (b) width of cracks 1, 5, 6 and 10.

5.3.2. Specimen C

The width vs loading F are plotted in Fig. 15 for the macrocrack and the four nearest cracks, namely from left to right: cracks 5, 6, 7 (macrocrack), 10 and 1 (see Fig. 13b). As can be seen in Fig. 15b, the widths of cracks 6 and 10 (closest to main crack) continued to increase after the peak, contrary to the widths of cracks 1 and 5. In this case also, the appearance of the macrocrack was sudden and its length was significant from the outset, as reported in the third row in Table 2. The rate of opening of the macrocrack was immediately higher than the other ones, thus showing that this crack behaved as a macrocrack at its earliest appearance. Its final width was 715 μm, that is 8.6 times greater than the final average width of the other cracks. This ratio

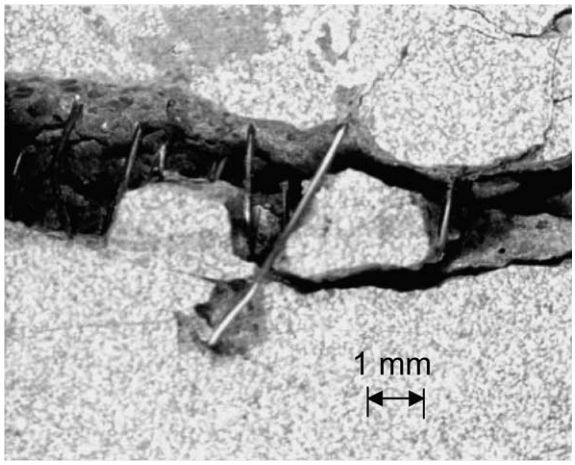

Fig. 16. Close-up view of macrocrack in specimen A after unloading.

is about five times lower than in the preceding case. This difference showed the influence of a modified cementitious matrix on the interaction between cracks.

5.3.3. Macrocrack

After unloading, the macrocrack remained open, while most of the other cracks could not be distiguished by the naked eye. Fig. 16 represents a close-up view of crack 17 after unloading of specimen A. It clearly shows that the residual opening of the macrocrack was due to the pull out of the steel fibres from the cementitious matrix. Keeping in mind that the peak of the loading curve was strongly related to the opening of the macrocrack, it might be expected that lower bond conditions between steel fibres and cementitious matrix involved lower peak-load and higher ductility. This was actually the case for specimen C.

5.4. Relation between opening and spacing of cracks

Valuable information about the multiple cracking process of cement-based composites may be derived from the analysis of the relation between spacing and opening of cracks. To this purpose, full-field measurement proves a powerful method, since all cracks may be precisely and easily taken into account. This is done in the present section for specimen A.

Let Δl define the mean distance between neighbouring cracks as follows (see Fig. 17):

$$\Delta l = \tfrac{1}{2}(l_l + l_r) \quad (1)$$

For the last crack on the left hand side of the central zone, $\Delta l = l_r$. For the last crack on the right hand side of the central zone, $\Delta l = l_l$.

Eq. (1) has been used to describe the distance between neighbouring cracks at the lowermost edge of specimen A. Δl vs crack location x is plotted in Fig. 18. As expected, Δl is randomly distributed along the beam. Within the zone under investigation, the average spacing

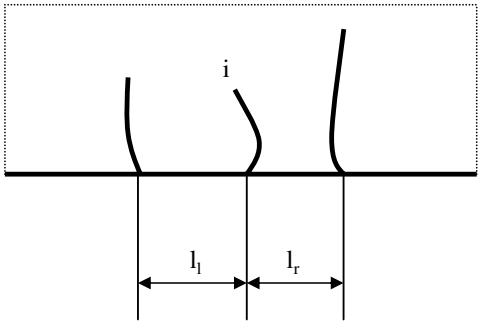

Fig. 17. Definition of Δl for crack i: $\Delta l = \frac{1}{2}(l_l + l_r)$.

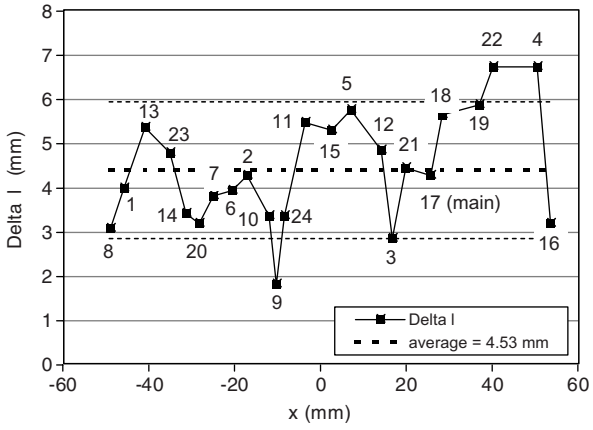

Fig. 18. Δl, specimen A.

$\overline{\Delta l}$ is equal to 4.53 mm with a standard deviation equal to 1.29 mm (see Table 3). Most Δl values lie between $2\overline{\Delta l}/3$ and $3\overline{\Delta l}/2$. From this point of view, the cracking behaviour of Material 1 could be compared to that usually observed for reinforced concrete [15].

Crack opening and crack spacing are interdependent variables which are randomly distributed along the bottom tensile face of specimens. The relationship between these two variables may be characterized by the ratio $k = w/\Delta l$, where w and Δl are related to each of cracks existing in the zone under investigation. This ratio is representative of the influence of crack spacing on crack opening. Values of ratio k have been estimated at the bottom edge of specimen A. They are plotted in Fig. 19 for $F = 71$ kN. The macrocrack is omitted, since its opening is of a higher magnitude (see Section 5.3.1). Here again, the distribution of k along the beam might

Table 3
Statistical analysis of the cracks, specimen A

	Average	Standard deviation	Coefficient of variation (%)
w	39 μm	16 μm	42
Δl	4.53 mm	1.29 mm	29
k	10.2 μm/mm	4.5 μm/mm	48

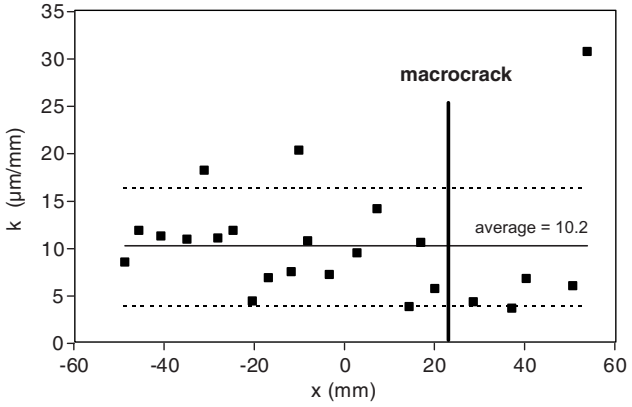

Fig. 19. $k = w/\Delta l$ vs x, specimen A.

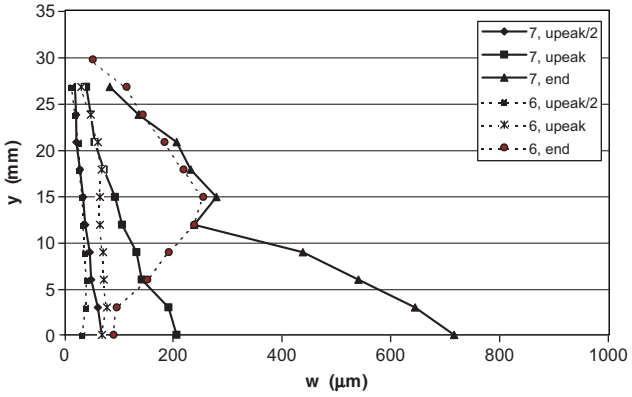

Fig. 21. w vs y, cracks 6 and 7 (macrocrack), specimen C.

be compared to that usually observed for reinforced concrete. It is worth noting that most k values range between $\bar{k}/3$ and $5\bar{k}/3$, with an average $\bar{k} = 10.2\,\mu m/mm$.

5.5. Profile of the cracks

The widths w of some cracks were measured through the depth of the beam and their evolutions were observed during the test. Typical results obtained for specimens A and C are plotted in Figs. 20 and 21. In both cases, the macrocrack and one of its two neighbouring cracks are considered at three loading stages: $u = u_{peak}/2$, $u = u_{peak}$ and at the end of the test. The increase in width of the macrocrack is clearly visible in both cases. The profile was approximately linear at $u = u_{peak}/2$ and at $u = u_{peak}$ whereas the width became more and more important near the bottom edge for both specimens A and C at the end of test. The height of the main crack increased at a constant rate in specimen A during the test, whereas it remained approximately constant in specimen C. The width of crack 18 in specimen A was less than the width of crack 6 in specimen C. This result is consistent with the remarks above (see Section 5.2.2) since the total number of cracks was lower in the second case. It is worth noting that the increase in width of macrocrack 7 at the bottom of specimen C was directly related to the decrease in width of its neighbouring crack 6. The phenomenon was probably due to the complex redistribution of the stress in the multi-cracked zone of the specimen during the second stage of the test, when the number of cracks increased.

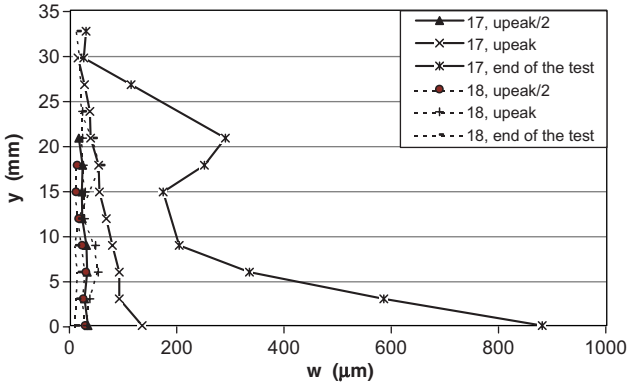

Fig. 20. w vs y, cracks 17 (macrocrack) and 18, specimen A.

6. Conclusions

The cracking process of beams made of a cement-based fibre composite has been studied. Beams were tested in three- or four-point bending. For one beam, the properties of the cementitious matrix had been purposely modified to influence its cracking response. The cracking morphology was observed and analysed by means of a full-field measurement technique. The following conclusions may be drawn from the present study.

Concerning the method of measurement used:

- Full-field measurement method has proved an efficient and powerful tool for extensive analysis of multiple cracking process.
- Existing cracks are revealed by discontinuities in the displacement field provided by the measurement method on the surface of the specimens.
- Early crack detection is made possible by means of this method: cracks need not be wider than about 9 µm for their detection.
- There is no need to anticipate locations of cracks for their measurement. Therefore, location, initial length and width can be easily and precisely determined for any new crack appearing within the zone under investigation.
- Propagation of existing cracks can be derived by comparing crack diagrams obtained at consecutive loading levels.

Concerning the cracking activity in the tested specimens:

- Multiple cracking has been observed for all specimens, including those tested in three-point bending. The evolution of the crack patterns has been precisely analysed by means of the full-field measurement method.
- Cracks did not appear or extend smoothly. Their initial length was usually immediately significant. This length increases with the loading force. Most of the cracks formed during the second stage of the *F*/*u* curve, before the load had reached its peak value.
- One of the cracks behaved as macrocrack as soon as it formed. Its appearance was sudden and its length was immediately significant. In the notched specimen, it formed in the notched cross-section. The main crack became a macrocrack when the peak-load was reached.
- In four-point bending, the cracks were randomly distributed along the specimens. In the notched specimens tested in three-point bending, they were concentrated around the mid-cross-section.
- Under similar test conditions, the total number of cracks in Material 2 was half that in Material 1. Besides, the crack opening increased in inverse proportion. This showed the influence of reduced bond conditions on the cracking morphology of the tested specimens.
- The full-field measurement method gives information on the profile of cracks. They usually exhibited a linear profile before peak-load. After the peak, the rate of macrocrack opening increased near the tensile edge of the specimens, whereas an opposite trend could be observed for some neighbouring cracks, showing an interaction between cracks.

Acknowledgments

The research reported in the current paper was supported by Lafarge. This company is gratefully acknowledged.

References

[1] Ammouche A, Riss J, Breysse D, Marchand J. Image analysis for the automated study of microcracks in concrete. Cement Concrete Compos 2001;23:267–78.
[2] Garcia D, Orteu JJ, Cutard T, Cailleux E. Application of stereovision to the mechanical characterization of refractory ceramics reinforced with metallic fibers. In: Conference on Experimental and Applied Mechanics, Milwaukee, WI, USA, 10–12 June 2002. Society for Experimental Mechanics; 2002.
[3] Aassved Hansen E. A holographic real time study of crack propagation in concrete. Cement Concrete Res 1989;19:611–20.
[4] Horii H, Ichinomiya T. Observation of fracture process zone by laser speckle technique and governing mechanism in fracture of concrete. Int J Fract 1991;51:19–29.
[5] Surrel Y. Moiré and grid methods: a signal-processing approach. Interferometry '94: photomechanics, published by Pryputniewicz RJ, Stupnicki J, volume 2342 de Proc Soc Photo-Opt lustrum Eng, 1994. p. 213–20.
[6] Périé J-N, Calloch S, Cluzel C, Hild F. Analysis of a multiaxial test on a C/C composite by using digital image correlation and a damage model. Exp Mech 2002;42(3):318–28.
[7] Dantu P. Étude des contraintes dans les milieux hétérogènes, Application au béton. Ann ITBTP 1958;11(121):57–67.
[8] He S, Feng Z, Rowlands RE. Fracture process zone analysis of concrete using moiré interferometry. Exp Mech 1997; 37(3):367–73.
[9] Surrel Y. Fringe analysis. In: Rastogi PK, editor. Photomechanics. Springer-Verlag; 1999. p. 57–104 [Chapter 3].
[10] Surrel Y. Design of algorithms for phase measurements by the use of phase stepping. Appl Opt 1996;35(1):51–60.
[11] Dufort L, Grédiac M, Surrel Y. Experimental evidence of the cross section warping in short composite beams under three point bending. Compos Struct 2001;51:37–47.
[12] Grédiac M, Dufort L. Experimental evidence of parasitic effects in the rail shear test on sandwich beams. Exp Mech 2002; 42(2):186–93.
[13] Brandt AM, Prokopski G. Critical values of stress intensity factors in mode ii in cementitious composites. J Mater Sci 1990;25:3505–10.
[14] Methods for crack opening displacement (COD) testing. 3D19, 1972. British Standard Institution.
[15] Ghali A, Favre R. Concrete structures: stresses and deformations. Chapman and Hall; 1986.